Thermal and Electron-Induced Reactions of Hydrazoic Acid (HN_3) Adsorbed on Gold and Ice

S. R. Carlo, Jessica Torres, and D. Howard Fairbrother*

Department of Chemistry, The Johns Hopkins University, 3400 North Charles Street, Baltimore, Maryland 21218

Received: October 27, 2000; In Final Form: April 16, 2001

The chemistry of hydrazoic acid (HN_3) on polycrystalline gold and amorphous ice was studied as a function of HN_3 exposure, temperature, and X-ray irradiation using reflection absorption infrared spectroscopy (RAIRS) and X-ray photoelectron spectroscopy (XPS). On Au, HN_3 was found to adsorb molecularly at 100 K. In contrast, at 100 K the reaction of HN_3 with ice was dominated initially by deprotonation and the formation of azide ions (N_3^-). At higher HN_3 exposures on ice, RAIRS data was consistent with molecular adsorption, although a distinct, more strongly bound molecular state was also observed that is attributed to hydrogen bonding between H_2O and HN_3. Annealing HN_3 adsorbed on Au resulted in predominantly molecular HN_3 desorption while in the HN_3/ice system molecular desorption was accompanied by the production of ammonium azide ($NH_4^+N_3^-$). In contrast, $NH_4^+N_3^-$ was not observed on the Au surface during annealing experiments. The formation of $NH_4^+N_3^-$ is postulated to derive from the reactions of NH radicals, formed as a result of NN−NH bond cleavage, within the adsorbate layer. In both the HN_3/ice and HN_3/Au systems, secondary electrons generated by X-ray irradiation induced $NH_4^+N_3^-$ formation and nitrogen desorption, which are consistent with the following net reaction: $4HN_{3(a)} \rightarrow NH_4^+N_{3(a)}^- + 4N_{2(g)}\uparrow$

I. Introduction

Free hydrazoic acid (HN_3) exists in two resonance structures consisting of three inequivalent nitrogen atoms:[1,2]

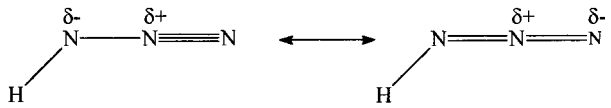

Hydrazoic acid is a moderately volatile (bp 37 °C), colorless, violently explosive liquid although the vapor can be handled at somewhat reduced pressure without difficulty. Hydrazoic acid has been used extensively in pyrolysis experiments and UV photolysis as a NH radical source that could ultimately be used as a low-temperature alternative to ammonia plasmas and in more efficient and higher power/energy hybrid electrochemical lasers.[3,4]

Hydrazoic acid is also a highly reactive nitriding agent whose reaction with a variety of semiconductor and metal surfaces has been the subject of a number of scientific investigations. Using high-resolution electron energy loss spectroscopy (HREELS), temperature-programmed desorption (TPD), and X-ray photoelectron spectroscopy (XPS), Chu et al. studied the hydrazoic acid-mediated nitridation of Si and GaAs.[5] At low exposures (<2 L) hydrazoic acid adsorbed molecularly on Si at 120 K and formed dimers at higher exposures (>2 L). Upon heating, HN_3 dissociated at ≈270 K, forming N_2 and NH, ultimately leading to the production of silicon nitride at $T > 1200$ K. On GaAs, 308 nm photons were used to photodissociate molecularly adsorbed HN_3 producing a mixture of NH_x, N_2, and N_3 species at 120 K. Subsequent surface annealing lead to nitridation of the GaAs. Similarly, Hemminger et al. have shown that HN_3 can act as a low-temperature nitriding agent in reactions with Ge(100).[6] Motivated by its potential importance in devices which require wide band gaps and high thermal conductivity, Russel et al. carried out a detailed investigation of Al nitridation using HN_3.[7] These results, combined with density-functional calculations,[8] TPD, and reflection absorption infrared results, indicate that HN_3 spontaneously dissociates upon adsorption at 100 K, producing N_2 and adsorbed NH groups. Above 200 K the NH groups decomposed, evolving molecular nitrogen.

The chemistry of HN_3 has also been studied on less reactive surfaces with a view toward surface modification. For example, using polarization-FT-infrared surface spectroscopy Heidberg et al. have shown that hydrazoic acid adsorbs molecularly on NaCl, decomposing under the influence of UV irradiation to form ammonium azide ($NH_4^+N_3^-$).[9] Thoms and Russel have reported that hydrogen azide adsorbs molecularly on hydrogenated diamond surfaces but decomposes on the bare C(100) surface to form carbon azide.[10] The driving force for this reaction was postulated to be the relative strength of the C−H bond vs the Si−H or Ge−H bonds which favors N−H rather than N−N bond cleavage.

In this study we report the results of an investigation on the interaction of hydrazoic acid (HN_3) with Au and ice surfaces. On Au, HN_3 was found to adsorb molecularly at 100 K. Upon annealing, HN_3 desorption is predominantly molecular. However, there is evidence of a more strongly bound chemisorbed HN_3 state which undergoes decomposition on the Au surface, ultimately leading to the production of a Au−N(H) bond at room temperature. On ice, the initial reaction of HN_3 leads to deprotonation and formation of azide ions (N_3^-). Higher HN_3 exposures lead to molecular adsorption, although a distinct, more strongly bound molecular state was observed that has been attributed to hydrogen bonding between H_2O and HN_3. Ammonium azide ($NH_4^+N_3^-$) was produced upon annealing the

* Author to whom correspondence should be addressed.

10.1021/jp003989k CCC: $20.00
Published on Web 06/09/2001

ice/HN_3 system and also following X-ray irradiation of the ice/HN_3 or Au/HN_3 systems, suggesting a common mechanism. The loss of nitrogen from the ice/HN_3 system during X-ray irradiation was found to be consistent with the net reaction: $4NH_{3(a)} \rightarrow NH_4^+N_{3(a)}^- + 4N_{2(g)}\uparrow$

II. Experimental Section

Low-temperature (≈100 K) experiments were carried out in an ultrahigh vacuum (UHV) chamber equipped with two UHV compatible leak valves for gas dosing, an ion gun for sample cleaning, a Physical Electronics 04-500 Dual Anode X-ray Source and 15-255 Precision Energy Analyzer, Balzers Prisma quadrupole mass spectrometer for gas analysis, and a custom-designed side-chamber for reflection absorption infrared measurements. The main chamber was pumped directly by a 200 L s^{-1} ion pump and the infrared side-chamber by a 75 L s^{-1} turbomolecular pump. In the absence of a system bakeout, this pumping arrangement allowed a base pressure of 1×10^{-8} Torr to be maintained. The interaction of HN_3 with Au at room temperature was studied using a Physical Electronics 04-500 Dual Anode X-ray Source, and 10-360 Precision Energy Analyzer described in more detail previously.[11,12]

During this investigation, polycrystalline Au (99.99%, Accumet) and similarly sized microscope slides with micron thick Au films were used as substrates. Samples were mounted on a copper sample holder attached to a ceramic feedthrough coupled to an UHV sample manipulator. Sample cooling was achieved by passing liquid nitrogen under pressure into a stainless steel tube connected to the ceramic feedthrough. This arrangement enabled temperatures of 90−100 K to be attained, as measured by a chromel−alumel thermocouple attached directly to the front face of the substrate. Sample heating was carried out by replacing the flow of liquid nitrogen with gaseous nitrogen. Au substrates were cleaned by sputtering with 4 kV Ar ions until judged clean by X-ray photoelectron spectroscopy (XPS).

Reflectance absorption infrared (RAIR) measurements were carried out using a Mattson Infinity Series FTIR spectrometer equipped with external beam capabilities. Experiments carried out in this investigation employed both indium antimonide (In−Sb) and narrow band, mercury−cadmium−telluride (MCT) detectors. The lower limit of the In−Sb detector was ≈1900 cm^{-1} and the MCT detector ≈750 cm^{-1}. Absorbance spectra were acquired by summing 32−250 sample scans when using the In−Sb detector and 125−1000 scans when using the MCT detector. RAIR Spectra were recorded using a resolution of 4 cm^{-1} and referenced to a clean Au surface.

X-ray photoelectron spectra were recorded with Mg Kα X-ray radiation (1253.6 eV) at 15 kV and 300 W, using a 45° takeoff angle with respect to the sample normal. Full surveys (binding energy = 600−50 eV) were measured with a pass energy of 200 eV and 0.5 eV/step. Elemental scans routinely employed a pass energy of 50 eV and 0.125 eV/step. Typical data collection times for the N(1s) region were 10 min. X-ray-induced reactions of HN_3 were monitored using the X-ray gun concurrently with data collection at a pass energy of 50 and 0.25 eV/step. Binding energy scales were referenced to literature values of the HN_3 bands[1,5] while the Au($4f^{7/2}$) peak[13] was used as a reference for any peak shifts observed during X-ray irradiation. XPS data fitting was performed with AugerScan software utilizing 100% Gaussian curves.[14]

Hydrazoic acid was prepared in a glass vacuum line under low vacuum conditions (≈300 mTorr), as the gas-phase effluent in the high temperature (≈390 K) reaction between sodium azide and a 10-fold excess of stearic acid. HN_3 gas was passed through a drying column to minimize water contamination and then trapped in a liquid-nitrogen-cooled stainless steel bulb connected to the glass line. The stainless steel container was subsequently removed from the glass line and attached to a gas dosing line connected to a UHV compatible leak valve. Hydrazoic acid gas purity was verified daily using the mass spectrometer (parent peak (HN_3^+), $m/e = 43$). To minimize contamination from leaks in the gas manifold, hydrazoic acid gas was trapped back into the sample cylinder at the end of each experiment.

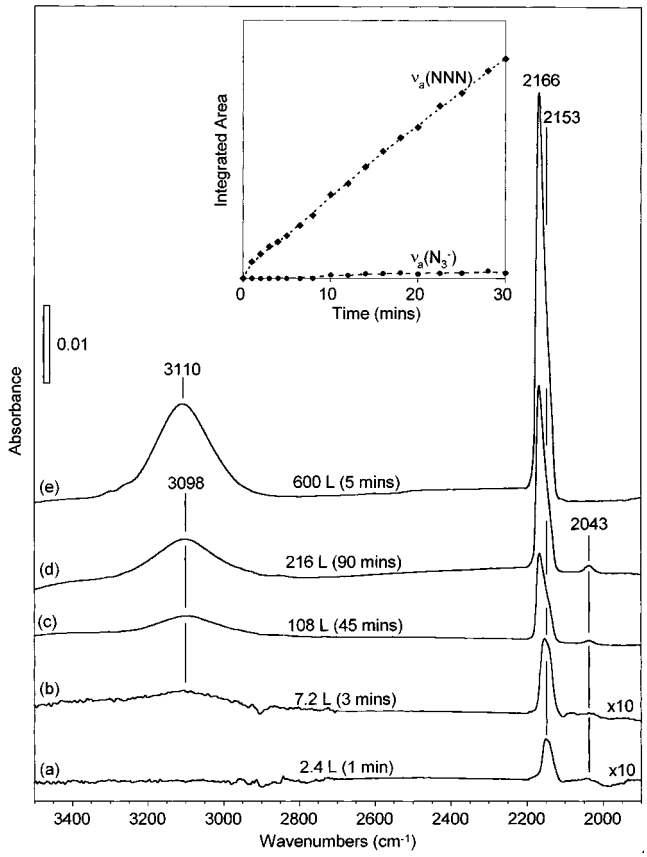

Figure 1. RAIR spectra as a function of HN_3 exposure time on Au at 100 K. Figures 1(a)−1(d) shows Au exposed to HN_3 at 4×10^{-8} Torr as a function of exposure time, while Figure 1(e) shows Au exposed to HN_3 at 2×10^{-6} Torr for 5 min. The region from 2200 cm^{-1} to 2700 cm^{-1} showed no features (except background CO_2) and has been removed from each data set for clarity. The inset shows the integrated areas of the υ_a(NNN) and $\upsilon_a(N_3^-)$ peaks at ≈2170 cm^{-1} and 2043 cm^{-1}, respectively, for the first 30 min of HN_3 exposure.

The H_2O used during the present investigation was Millipore filtered and subjected to several freeze−pump−thaw cycles prior to use. D_2O (Aldrich, 100 atom %) was used without filtering. Ice films were prepared by exposing Au substrates at 90−100 K to water vapor introduced into the chamber through a UHV compatible leak valve.

III. Results

HN_3/Gold. Figure 1 shows the RAIRS spectra of a polycrystalline Au sample held at 100 K as a function of HN_3 exposure time ($P_{HN_3} = 4 \times 10^{-8}$ Torr). A comparison of RAIRS results from this work and literature IR band assignments for gas-phase and adsorbed HN_3 are shown in Table 1. Initially, two bands appear in the RAIR spectra centered at 2153 cm^{-1} and 3098 cm^{-1} which can be identified as the asymmetric bending mode, υ_a(NNN), and symmetric stretching mode,

TABLE 1: Summary of Previous IR Work (>1100 cm^{-1}) on Hydrazoic Acid Showing Normal Mode Frequencies for HN_3 in the Gas Phase, a Nitrogen Matrix, and Adsorbed on Al(111) (In this table physisorbed refers to monolayers one and two, and condensed to the multilayer regime.) All values are in wavenumbers (cm^{-1})

mode	gas	physi-sorbed	con-densed	N_2 matrix	this work
υ_s(N−H)	3324[7] 3497[16,17] 3408[44] 3339[19,26]	3220[7] 3340[45]	3120[7]	3324[16,17]	3098−3120
υ_a(NNN)	2150[7] 2140[16,17] 2137[19,26]	2160[7]	2155[7] 2140[18 a]	2150[16,17]	2140−2153 2163−2177
δ_s(NH)	1273[7] 1265[16,17] 1266[19,26]	1310[7]	1277[7] 1269[18]	1273[16,17]	1306
υ_s(NNN)	1168[7] 1151[16,17] 1153[19,26]	1200[7] 1270[45]	1189[7] 1269[18 a]	1168[16,17]	1205
$\upsilon_s + \upsilon_a$(NNN)	3318[7] 3291[16,17] 3290[19,26]	3360[7]	3344[7] 3409[18*]	3318[16,17]	3302

[a] Solid sample.

υ_s(N−H), of HN_3, respectively.[5,7,8,15−19] After 8 min HN_3 exposure, the υ_a(NNN) band broadened and the peak maximum shifted to 2166 cm^{-1}. At longer HN_3 exposure times (>10 min) another peak at 2043 cm^{-1} was observed concomitant with the appearance of a small broad band at ≈3400 cm^{-1}, the latter due to υ_s(O−H) of adsorbed water.[20] This new feature at 2043 cm^{-1} can be identified as the antisymmetric bending mode of the azide anion, $\upsilon_a(N_3^-)$.[18,21] *Hereafter to differentiate modes due to molecular hydrazoic acid and the azide ion, υ(NNN) refers to hydrazoic acid and υ(N_3^-) to the corresponding NNN mode of the azide ion.* The inset in Figure 1 shows the integrated areas of the υ_a(NNN) band at 2153 cm^{-1} and the $\upsilon_a(N_3^-)$ band at 2043 cm^{-1} as a function of HN_3 exposure. Figure 1(e) shows the RAIR spectra of a polycrystalline Au substrate exposed to ≈600 L of HN_3 over a period of 5 min. In the context of Figure 1(a)−1(d) this corresponds to a total exposure time of 200 min. In contrast to Figure 1(a)−1(d), only IR peaks due to molecular HN_3 were observed (i.e., no spectral intensity associated with the azide ion at 2043 cm^{-1} was detected in Figure 1(e)).

Figure 2 shows the RAIR spectra of a gold substrate exposed to 110 L of HN_3 at 90 K, as a function of temperature. The υ_s(N−H) band present at 3120 cm^{-1} is sharper than was observed in Figure 1. The reason for this discrepancy is unclear but is at least consistent with a difference in the actual surface temperature between Figure 1 and Figure 2. This is supported by a previous investigation by Dows et al.[15] on the IR spectrum of solid hydrazoic acid, which revealed that an irreversible phase transition occurs on warming solid hydrazoic acid above ≈120 K accompanied by a sharpening of the υ_s(N−H) band, similar to the difference observed between Figure 1 and Figure 2. Apart from minor shifts in peak positions (ascribed to the effect of differences in film thickness) the only feature not observed in Figure 1 is the peak at 3302 cm^{-1}. This feature has been previously identified as a combination mode of υ_s(NNN) and υ_{as}(NNN).[16]

At a surface temperature of 130 K (Figure 2(d)) no spectral intensity remained for the υ_s(N−H) mode at 3120 cm^{-1}. In addition a small peak at 2140 cm^{-1} was evident in the υ_a(NNN) region as well as a feature at 2043 cm^{-1} due to azide ions. The inset in Figure 2 shows the integrated areas for the υ_a(NNN) and $\upsilon_a(N_3^-)$ bands between 90 and 170 K. In contrast to the υ_s(N−H) and υ_a(NNN) modes the $\upsilon_a(N_3^-)$ band intensity actually increased slightly above 100 K. Both of the bands at 2043 and 2140 cm^{-1} could be observed in the RAIR spectra until a surface temperature of ≈170 K was reached. Above this temperature no IR peaks due to adsorbate molecules were observed.

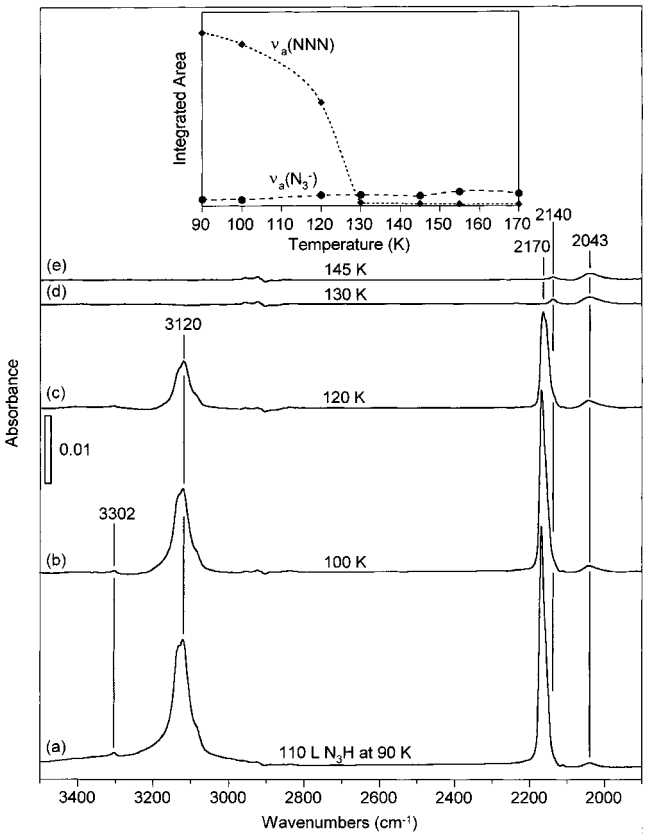

Figure 2. RAIR spectra of a Au substrate exposed to 110 L HN_3 dose as a function of surface temperature. The inset shows the integrated areas of the υ_a(NNN) and $\upsilon_a(N_3^-)$ peaks at ≈2170 cm^{-1} and 2043 cm^{-1}, respectively, as a function of surface temperature. The region from 2200 cm^{-1} to 2800 cm^{-1} showed no features (except background CO_2) and has been removed from each data set for clarity.

Figure 3 shows the RAIR spectra of 150 L HN_3 adsorbed on gold at 100 K (a) initially, and (b) following 210 min of 300 W X-ray irradiation. Adsorbed HN_3 is clearly susceptible to X-ray-induced chemistry, evidenced by the loss of υ_a(NNN) and υ_s(N−H) band intensities at 2163 and 3120 cm^{-1}, respectively. The small band at 2145 cm^{-1} (Figure 3(b)) remaining after irradiation probably arises from unreacted hydrazoic acid. X-ray irradiation also leads to the observation of new IR peaks centered at 2076 cm^{-1}, 2855 cm^{-1}, 3050 cm^{-1}, 3150 cm^{-1}, and 3355 cm^{-1} (Figure 3(b)). Based on previous studies by Pimental et al.[21] and Gray and Waddington,[18] these modes are diagnostic of ammonium azide ($NH_4^+N_3^-$). A comparison of RAIRS results from this work and literature IR band assignments for $NH_4^+N_3^-$ and N_3^- are shown in Table 2.

In Figure 3, the N(1s) XPS data (corresponding to the RAIR spectra in Figure 3(a) and 3(b)) are shown as insets. The N(1s) spectra of the parent HN_3 molecule adsorbed on Au at 100 K (Figure 3(a) and inset) was fitted with the following parameters:[2,22] NN*N*H: 399.9 eV, 31.6%; *N*NNH: 400.8 eV, 31.6%; N*N*NH: 404.0 eV, 36.8%. Following irradiation the N(1s) spectra exhibited poorer signal-to-noise consistent with significant X-ray-induced nitrogen desorption. Despite the weaker overall spectral intensity, however, the N(1s) region has clearly

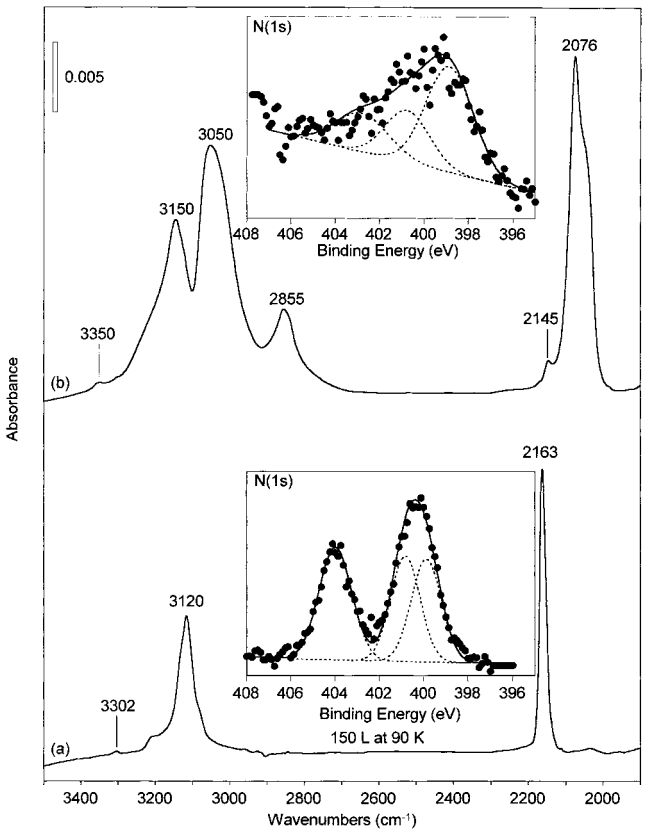

Figure 3. RAIR spectra of a Au substrate exposed to 150 L HN_3 dose at 90 K (a) before and (b) following 210 min exposure to 300 W, Mg Kα X-ray irradiation. The insets show the corresponding N(1s) XPS data recorded with a pass energy of 25 eV, fitted to (a) HN_3 and (b) $NH_4^+N_3^-$. Details of the fitting parameters can be found in the text. Note that due to the poor signal-to-noise the XPS data set fitted to $NH_4^+N_3^-$ has been smoothed.

TABLE 2: Comparison of Published IR Assignments (>1100 cm^{-1}) for N_3^- and $NH_4^+N_3^-$ with Results from the Present Investigation (All values are in wavenumbers (cm^{-1}))

mode	N_3^- azide ion refs 16,21,46	$NH_4^+N_3^-$ Pimental et al. ref 21	$NH_4^+N_3^-$ Gray & Waddington ref 18	$NH_4^+N_3^-$ this work
unknown	N/A	1200	N/O	N/O
ν_s(NNN)	1350[a]	1345 (ν_2')	N/O	N/O
δ_a(N−H)	N/A	1420−1440 (ν_2) 1671 (ν_4)	1414 (ν_4^+)	1430
unknown	N/A	N/O	1709 (ν_2^+)	N/O
comb.	N/A	1830−1850 ($\nu_4+\nu_6$)	1818 ($\nu_4+\nu_6$)	1836
ν_a(NNN)	2240 2040 2075[a]	2030−2050 (ν_1')	2041 (ν_3^-)	2043−2076
comb.	N/A	2270 ($\nu_4+2\nu_6$)	N/O	N/O
ν_s(N−H)	N/A	3160 (ν_3B or $\nu_2+\nu_4$) 3040 (ν_3A)	3100−2941 (ν_3^+)	3143−3151 3024−3050
		2880 (ν_3B or $2\nu_4$)	2817 ($2\nu_4^+$)	2855−2864
comb.	N/A	3355 ($\nu_1'+\nu_2'$)	N/O	3350

[a] Calculated values.

changed compared to the parent HN_3 spectra and can be qualitatively fitted to $NH_4^+N_3^-$ (*NNN*$^-$: 398.7 eV, 52.1%; *N*H_4^+: 400.7 eV, 25.8%; N*NN*$^-$: 402.7 eV, 22.1%). A comparison of the N(1s) XPS peak positions used for HN_3 and $NH_4^+N_3^-$ in this work and previous studies is shown in Table 3.

TABLE 3: Comparison of N(1s) XPS Peak Positions Used Previously for Hydrazoic Acid (HN_3) and the Azide Ion (N_3^-) with Equivalent Peak Positions from This Investigation (All values are quoted in eV)

N species	ref 22	ref 2	this work
*N*NNH	399.8	399.7	401.5
N*N*NH	404.1	403.6	404.1
NN*N*H	400.8	399.7	400.3
N*N*N$^-$	403.4	402.3	402.9−403.5
NNN$^-$	399.0	398.0	399.0
NH_4^+	N/A	400.3	401.0

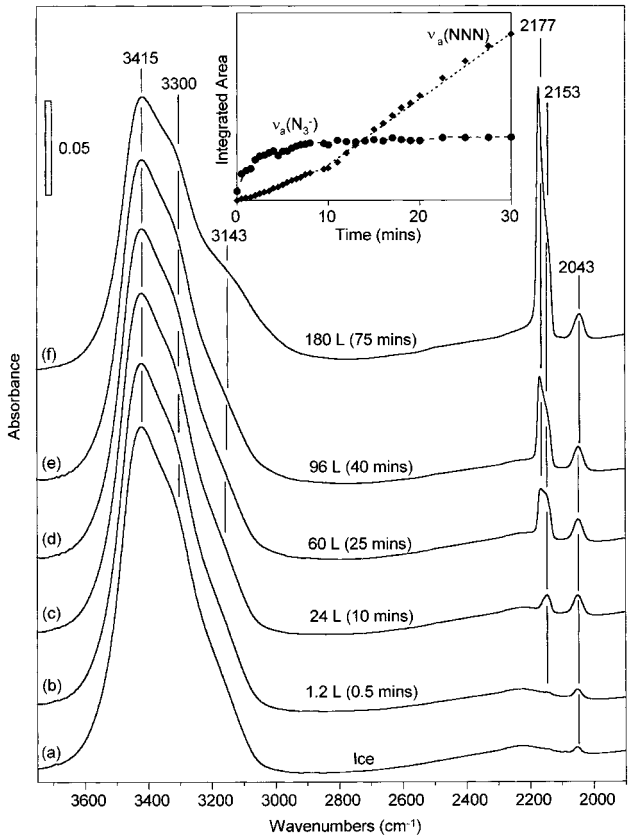

Figure 4. Variation in RAIR spectra as a function of HN_3 exposure ($P_{HN_3} = 4 \times 10^{-8}$ Torr) onto an ice film deposited at 100 K. The inset shows the integrated areas of the ν_a(NNN) and $\nu_a(N_3^-)$ peaks present at ≈2170 cm^{-1} and 2043 cm^{-1}, respectively, as a function of HN_3 exposure time. The region from 2200 cm^{-1} to 2800 cm^{-1} showed no features (except background CO_2) and has been removed from each data set for clarity.

HN_3/Ice. An amorphous ice film[20,23] deposited at $T \leq 100$ K, was exposed to HN_3 at 4×10^{-8} Torr for 75 min and RAIR spectra recorded as a function of HN_3 exposure time. The results of this experiment are shown in Figure 4. Initially, the ice film showed a broad band centered at 3415 cm^{-1} with two shoulders of lower intensity at ≈3300 cm^{-1} and ≈3200 cm^{-1}, consistent with previous IR studies of low-temperature H_2O films.[23,24] A smaller band was also visible at 2043 cm^{-1}. On the basis of previous literature assignments and information contained in Figures 1−3, this feature at 2043 cm^{-1} can be identified as $\nu_a(N_3^-)$.

Following HN_3 exposure to the ice film the $\nu_a(N_3^-)$ band at 2043 cm^{-1} continued to grow in intensity. During this initial interaction between HN_3 and the amorphous ice film, IR spectral intensity was also observed in the ν_a(NNN) region centered at

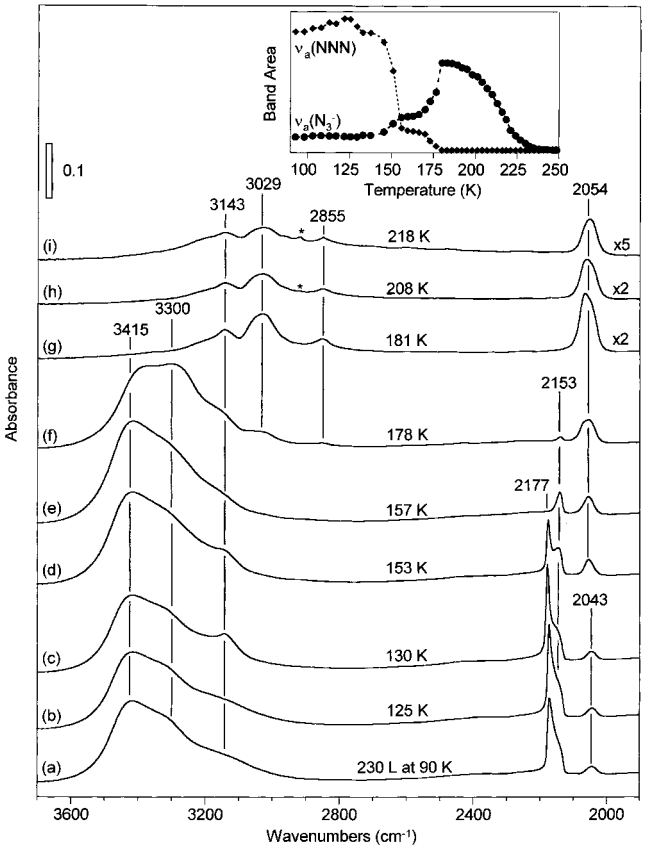

Figure 5. RAIR spectra of an ice film following a 230 L exposure of HN_3 as a function of temperature. The inset shows the integrated areas of the υ_a(NNN) parent and $\upsilon_a(N_3^-)$ peaks present at ≈2170 cm^{-1} and 2043 cm^{-1}, respectively, as a function of temperature. The starred (*) band present at ≈2900 cm^{-1} is due to hydrocarbon impurities adsorbed from the background. The region from 2200 cm^{-1} to 2800 cm^{-1} showed no features (except background CO_2) and has been removed from each data set for clarity.

2153 cm^{-1}. At longer HN_3 exposure times (>10 min) a second band was observed at 2177 cm^{-1} corresponding to υ_a(NNN) of the condensed multilayer. A broad υ_s(N−H) stretching mode, visible in the difference spectrum was also observed at approximately 3143 cm^{-1}. The inset in Figure 4 shows the integrated areas of the υ_s(NNN) and $\upsilon_a(N_3^-)$ bands as a function of HN_3 exposure time.

Following a 230 L HN_3 exposure to an ice film at 100 K the surface was warmed by replacing the flow of liquid N_2 with N_2 gas. The evolution of the HN_3/ice film as a function of temperature is shown in Figure 5. At 130 K (Figure 5(c)) the υ_s(N−H) band at 3143 cm^{-1} sharpened, consistent with changes in the IR spectra that have been observed to accompany the irreversible phase change within solid HN_3.[15] Between 130 K and 157 K, the spectral intensity in the υ_a(NNN) could be resolved into two components centered at 2177 cm^{-1} and 2153 cm^{-1}. The feature at 2177 cm^{-1} decreased rapidly in intensity with increasing surface temperature and completely disappeared by ≈157 K. In contrast the 2153 cm^{-1} feature exhibited greater thermal stability and was observable in the RAIR spectrum until a surface temperature ≈181 K was reached. Above 157 K, bands were observed at 3143 cm^{-1}, 3029 cm^{-1}, and 2855 cm^{-1}. These new IR bands observed are indicative of ammonium azide, ($NH_4^+N_3^-$) formation.[18,21] Between 157 K and 178 K a reversal in the intensity pattern of the 3415 cm^{-1} and 3300 cm^{-1} O−H stretching bands was also observed, consistent with a phase change within the film.[24] Between 78 K and 181 K, ice desorbed from the surface, evidenced by the absence of vibrational

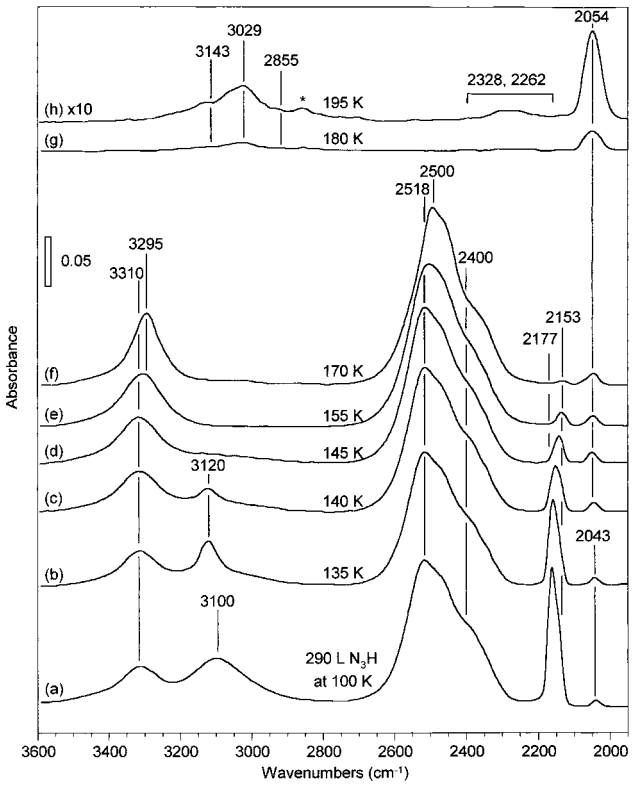

Figure 6. RAIR spectra of (a) H_2O/D_2O film, (b) the same H_2O/D_2O film following exposure to 290 L HN_3 at 100 K, and (c)−(i) as a function of temperature. The starred (*) band at ≈2900 cm^{-1} is due to hydrocarbon impurities adsorbed from the background.

intensity in the O−H stretching region. Above 181 K only bands associated with ammonium azide at 3143 cm^{-1}, 3029 cm^{-1}, and 2855 cm^{-1}, and the $\upsilon_a(N_3^-)$ band at 2054 cm^{-1} remained (Figure 5(g)). Ammonium azide bands remained until a surface temperature of ≈230 K was reached. The inset to Figure 5 shows that the increase in intensity of the $\upsilon_a(N_3^-)$ bands at ≈150 K and 175 K are correlated with losses in the υ_a(NNN) band intensity.

To further clarify the nature of the reactions occurring within the ice/hydrazoic acid films, additional RAIRS experiments were carried out using an ice film composed mainly of D_2O (some H_2O was also observed due to adsorption of background gases). Results from this experiment are shown in Figure 6. Prior to HN_3 adsorption, spectral intensity was observed between 3150−3500 cm^{-1} and 2250−2700 cm^{-1} due to the υ(O−H) and υ(O−D) stretching modes of adsorbed H_2O and D_2O, respectively, at 100 K. Following a 290 L exposure of HN_3 at 100 K, additional peaks centered at 3100 cm^{-1}, 2177 cm^{-1}, and 2043 cm^{-1} were observed. The peaks at 3100 cm^{-1} and 2177 cm^{-1} have previously been identified with the N−H stretching and NNN asymmetric stretching modes of molecular hydrazoic acid, respectively,[15] while the 2043 cm^{-1} mode is due to the $\upsilon_a(N_3^-)$ band of azide ions.[21] The initial peak profile of the υ_a(NNN) band at 100 K is similar to that observed for HN_3 adsorbed on a pure H_2O ice film (Figure 5), with a peak maximum at 2177 cm^{-1} and a lower frequency shoulder centered at approximately 2153 cm^{-1} (compare Figures 5(a) and 6(a)).

For the IR modes associated with HN_3 and N_3^-, the evolution of the RAIR spectrum as a function of increasing film temperature was qualitatively similar to that observed in Figure 5. Thus by 135 K the υ_s(N−H) band sharpened (Figure 6(c)), consistent with the irreversible phase change observed in HN_3.[15] Similarly the loss of molecular HN_3 above 135 K was

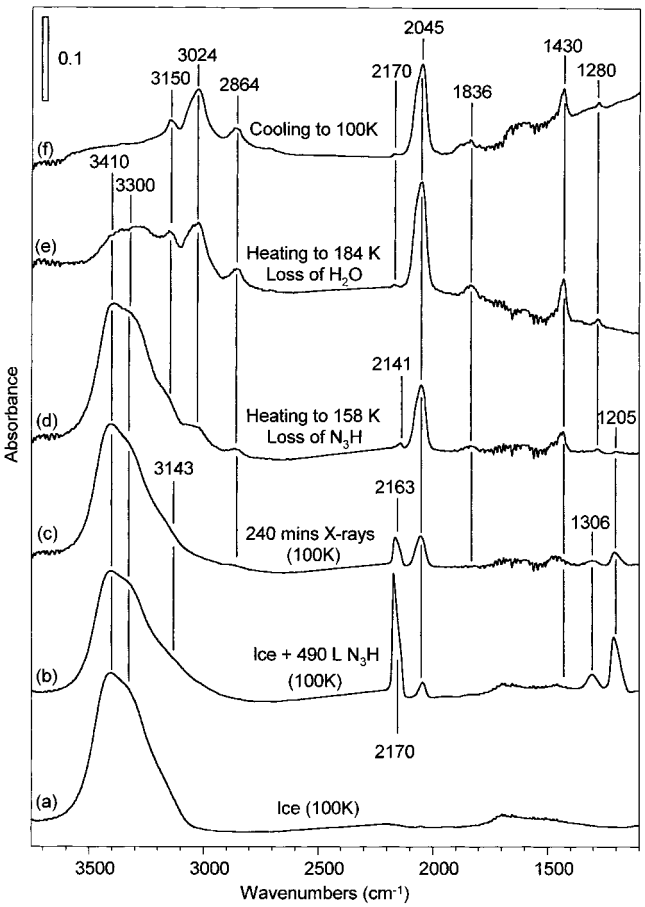

Figure 7. RAIR spectra recorded using a MCT detector of a 490 L HN_3 dose on ice, before and after X-ray irradiation followed by annealing to the temperatures indicated. Figure 7(f) was obtained by heating the X-ray-modified film to approximately 185 K before re-cooling to 100 K. The region from 2200 cm^{-1} to 2800 cm^{-1} showed no features (except background CO_2) and has been removed from each data set for clarity.

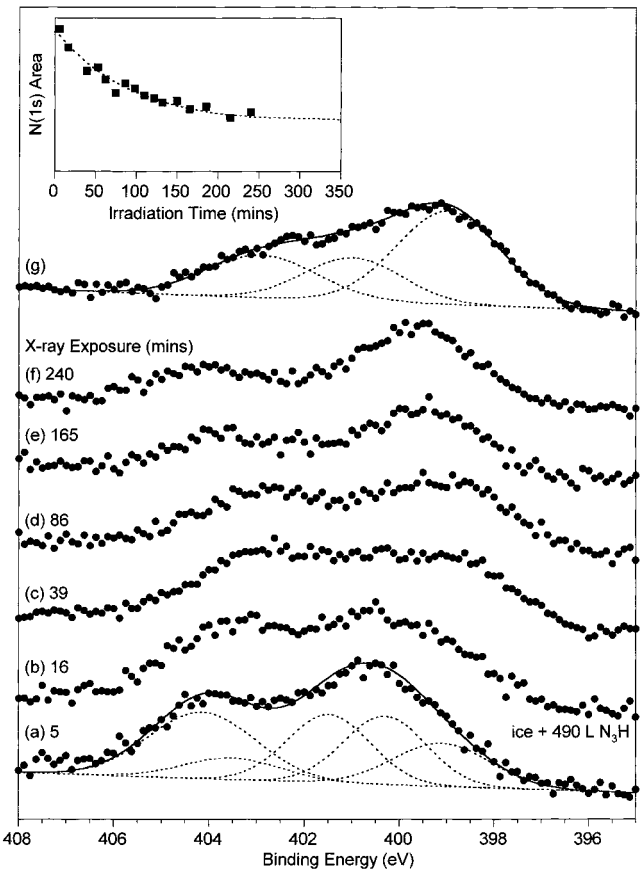

Figure 8. N(1s) XPS data corresponding to the RAIRS data shown in Figure 7: (a) following a 490 L HN_3 exposure to an ice film, (b)−(f) as a function of X-ray irradiation time, and (g) after X-ray irradiation and then annealing to 185 K followed by cooling to 100 K. The inset shows the area of the N(1s) region as a function of irradiation time. The dotted lines correspond to the best fit obtained using the functional form $[N]_t = 1/3 \times [N]_0 \times (2e^{-4k_{eff}t} + 1)$ where $k_{eff} = 0.162$ min^{-1}. Details of the fits to Figures 8(a) and 8(g) can be found in the text.

accompanied by a downshift in the υ_a(NNN) peak position and an increase in the $\upsilon_a(N_3^-)$ band intensity (Figure 6(d)−(g)). New IR peaks at 3143 cm^{-1}, 3029 cm^{-1}, and 2855 cm^{-1} also appeared above 180 K, consistent with the production of ammonium azide. In contrast to Figure 5, a new broad IR feature was also observed between 2450 cm^{-1} and 2200 cm^{-1} at temperatures above 180 K. This observation of RAIRS intensity between 2450−2200 cm^{-1} above 180 K is consistent with the formation of N−D bonds within ammonium azide (e.g., $NH_3D^+N_3^-$).[25] This assumption is also supported by the fact that this new IR feature exhibits similar thermal stability to that observed for $NH_4^+N_3^-$, disappearing by 230 K.

Figure 7 shows the RAIR spectra of 490 L HN_3 deposited on an amorphous ice film at 100 K, following X-ray irradiation and subsequent annealing. Analogous to the situation on Au (Figure 3), HN_3 adsorbed on ice also reacted during X-ray irradiation, evidenced by the loss of υ_a(NNN) band intensity at 2170 cm^{-1}. $NH_4^+N_3^-$ production during X-ray irradiation is evidenced by the appearance of N−H stretching and bending modes observed at 3150 cm^{-1}, 3024 cm^{-1}, 2864 cm^{-1}, and 1430 cm^{-1} (Table 2).[18,21] Similarly, the increase in intensity at 2045 cm^{-1} observed in Figure 7(c) following exposure to X-ray irradiation can be ascribed to N_3^- species associated with $NH_4^+N_3^-$ (Table 2). Following irradiation, the X-ray-modified film was heated and changes monitored using RAIRS. Annealing to 158 K caused further loss in HN_3 peaks and an increase in intensity due to bands previously assigned to $NH_4^+N_3^-$. Continued heating to 184 K resulted in a loss of adsorbed water, although modes due to $NH_4^+N_3^-$ remained. Upon subsequent cooling to 100 K only RAIRS bands previously assigned to $NH_4^+N_3^-$ were resolved.

Figure 8 shows the evolution of the N(1s) spectral envelope following a 490 L HN_3 exposure to an ice film and subsequent X-ray irradiation and annealing, corresponding to the RAIRS data shown in Figure 7. In accordance with RAIRS data the best fit to the N(1s) spectral envelope shown in Figure 8(a) consists of approximately 75% HN_3 (NN*N*H: 400.3 eV, 22.9%; *N*NNH: 401.5 eV, 22.9%; N*N*NH: 404.1 eV, 28.8%) and 25% N_3^- (*NNN*: 399.1 eV, 16.9%; N*N*N: 403.5 eV, 8.5%).[1,2,5] During X-ray irradiation the N(1s) envelope broadened at intermediate times ($\approx$ 40 min, Figure 8(c)) before sharpening again after prolonged exposures (Figure 8(d)−(f)). Following 240 min of irradiation the sample was warmed to 184 K before recooling to 100 K. Figure 8(g) shows the resulting N(1s) XPS spectra corresponding to Figure 7(f) fitted to $NH_4^+N_3^-$ (*NNN*$^-$: 399.0, 51.3%; *N*H$_4^+$: 401.0, 23%; N*N*N$^-$: 402.9, 26%). For the HN_3/ice film, the inset in Figure 8 shows the decrease in N(1s) XPS area as a function of X-ray irradiation time.

IV. Discussion

As a result of the heating arrangement, HN_3 molecules desorbed from the sample manipulator during annealing experiments, typically approaching a maximum pressure of 1×10^{-6}

Torr. To examine the possible effect of background HN_3 on RAIRS measurements, separate experiments were carried out in the IR compartment using $P_{HN_3} \approx 1 \times 10^{-5}$ Torr with the Au substrate held at room temperature to prevent molecular adsorption. In the course of these experiments no gas-phase bands were observed in the υ_a(NNN) region. This observation allows us to be confident that bands observed in RAIRS experiments were due to adsorbate rather than gas-phase species, e.g., 2140 cm^{-1} assigned to υ_a(NNN) in Figure 2. Similarly the heating rates varied considerably. Consequently, changes in RAIR spectra were observed at different temperatures in separate experiments, although relative spectral changes remained consistent. As a result, no attempt has been made to determine adsorption/desorption enthalpies or surface energetics in the present investigation.

To examine any possible effects due to stray electrons, the RAIR spectra of a 250 L HN_3 film adsorbed on Au at 100 K was examined as a function of time. Results from this study revealed that the RAIR spectrum was unchanged over a period of 120 min, indicating that any changes in the overlayer observed in the present investigation can be ascribed either to the effect of X-ray irradiation or sample warming.

HN_3 Adsorption on Gold. In Figure 1 the observation of IR bands at ≈3110 cm^{-1} and ≈2160 cm^{-1} which can be ascribed to υ_s(N−H) and υ_a(NNN) indicate that the interaction of HN_3 with Au at 100 K leads to molecular adsorption.[5,7,8,16−19] This assertion is supported by the fact that the N(1s) XPS spectrum obtained under identical deposition conditions (Figure 3) can be fitted by three peaks of nearly identical area with peak positions in good agreement with literature values of HN_3.[2,22] The υ_s(N−H) mode is significantly red-shifted compared to the gas phase value due to hydrogen bonding between HN_3 molecules within the film,[7,27] while the coverage-dependent blue shift in υ_a(NNN) is consistent with the results of Russell et al. and can be rationalized in terms of the combined effects of both chemical and dipole−dipole interactions between adsorbate molecules.[7,28]

The formation of adsorbed azide ions in Figure 1 can be explained by the reaction of HN_3 with background water:

$$HN_{3(a)} + H_2O_{(a)} \rightarrow N^-_{3(a)} + H_3O^+_{(a)} \qquad (1)$$

This is supported by the appearance of azide ions on the gold surface concomitant with the observation of adsorbed water at ≈3400 cm^{-1} (Figure 1(e)). This assertion is also consistent with results of Figure 1(e) demonstrating that a large HN_3 exposure (600 L) carried out over a short time period, where adsorption of background water will be minimized, resulted in no azide ion formation.

Thermal Chemistry of HN_3 Adsorbed on Au. Figure 2 shows that the thermal chemistry of HN_3 adsorbed on Au is dominated by molecular desorption of the parent molecule at 130 K, consistent with thermal desorption data presented by Russel et al. who showed that desorption occurred at 130 K on Al(111).[7] Above this temperature, the observation of a RAIRS peak at 2043 cm^{-1} (Figure 2(d) and (e)) implies the presence of a more strongly bound chemisorbed HN_3 state in addition to adsorbed of $N_{3(a)}$. It should also be noted that no evidence of ammonium azide formation was observed in any thermal chemistry studies of HN_3 adsorbed on Au.

The results of this investigation do not allow us to unambiguously determine the subsequent thermal reactions of the more strongly bound nitrogen-containing moieties. However, the observation of a Au−N(H) bond observed as a peak centered at 398.2 eV in the N(1s) XPS spectra, following prolonged (60 min at 5×10^{-7} Torr) room-temperature exposure of Au to HN_3, indicates that HN_3 can be used as a low-temperature nitrogenating agent. One possible mechanism, consistent with our observations, involves the formation of AuN_3 and subsequent decomposition to AuN:

$$Au_{(s)} + HN_{3(g)} \rightarrow AuN_{3(s)} + {}^1/_2H_{2\,(g)}\uparrow \qquad (2)$$

$$AuN_{3(s)} \rightarrow AuN_{(s)} + N_{2(g)}\uparrow \qquad (3)$$

Gold azide (AuN_3) production could, in principle, arise from either chemisorbed HN_3 or $N^-_{3(a)}$. AuN_3 has been previously observed by XPS as one product in the reaction of azide ions with Au electrodes.[29] AuN_3 is believed to possess a large degree of covalent character[29] (Au−N=N^+=N^-) in contrast to the better known azides formed with more electropositive elements such as sodium (Na^+N^-=N^+=N^-). Subsequent thermal decomposition of AuN_3 is postulated to produce AuN (reaction 3).

X-ray-Induced Chemistry of Adsorbed HN_3 on Au. The interaction of X-rays with solid substrates is expected to produce a broad distribution of secondary electrons. Based on previous studies of X-ray-induced modification of fluoropolymers[30,31] and fluorine-containing organic thin films,[12,32] the X-ray-induced reactivity of adsorbed HN_3 can be reasonably assumed to arise from the interaction of these secondary electrons with the adsorbate.

RAIRS data from Figures 3 and 7, coupled with the N(1s) XPS data shown in Figure 8 support the idea that the sole product of X-ray irradiation of HN_3 adsorbed on either Au or ice surfaces is ammonium azide ($NH_4^+N_3^-$). Further evidence for $NH_4^+N_3^-$ formation is provided by the observed sublimation temperature of 230 K (determined from the disappearance of the infrared modes associated with ammonium azide in Figure 5). This value is in excellent agreement with infrared and mass spectrometer measurements by Heidberg et al. who examined the thermal stability of ammonium azide formed under vacuum conditions during UV irradiation of HN_3 adsorbed on NaCl-(100).[9] Furthermore, the observed changes in the N(1s), XP spectra of a HN_3/ice film during X-ray irradiation (Figure 3, inset), specifically the broadening of the N(1s) spectral envelope and an increase in the relative intensity at ≈398.5 eV (Figure 8(a)−(f)), can be qualitatively explained by conversion of HN_3 into $NH_4^+N_3^-$ (Figure 3, inset, and Figure 8(g)).

Mechanism of Ammonium Azide ($NH_4^+N_3^-$) Formation. Adsorbed HN_3 has previously been reported to transform into ammonium azide[9,33] under the influence of UV irradiation. Based on these observations, the initial step in $NH_4^+N_3^-$ formation during X-ray irradiation is hypothesized to involve the production of NH radicals by electron impact dissociation of HN_3, which have previously been identified as products in the electron beam dissociation of gas-phase HN_3:[4,34,35]

$$HN_{3(a)} + e^- \rightarrow\rightarrow NH(A^3\Pi, c^1\Pi)_{(a)} + N_{2(g)}\uparrow \qquad (4)$$

Subsequent abstraction reactions between NH radicals and adsorbed HN_3 molecules lead to NH_3 production, whose reaction with HN_3 yields $NH_4^+N_3^-$. A possible reaction mechanism is proposed below:

$$NH_{(a)} + HN_{3(a)} \rightarrow NH_{2(a)} + N_{3(a)} \qquad (5)$$

$$NH_{2(a)} + HN_{3(a)} \rightarrow NH_{3(a)} + N_{3(a)} \qquad (6)$$

$$HN_{3(a)} + NH_{3(a)} \rightarrow NH_4^+N^-_{3(a)} \qquad (7)$$

Molecular nitrogen is released as a result of bimolecular collisions between N_3 groups:

$$2N_{3(a)} \rightarrow 3N_{2(g)}\uparrow \quad (8)$$

The overall reaction stoichiometry is thus:

$$\textit{Net}: 4HN_{3(a)} \rightarrow NH_4^+N_{3(a)}^- + 4N_{2(g)}\uparrow \quad (9)$$

Support for this mechanism is also provided by the observation of NH_3 and N_2 in reaction studies of NH radicals, generated from the UV photolysis of HN_3, with alkenes.[36,37]

Kinetics of X-ray-Induced Ammonium Azide Formation. On the basis of the proposed mechanism, combined with the low or zero activation energies that accompany most free radical reactions, it is reasonable to assume that the rate-limiting step in $NH_4^+N_3^-$ formation will be the initial production of NH radicals, mediated by the influence of X-ray generated secondary electrons: [34]

$$HN_{3(a)} \xrightarrow{k_{eff}} NH_{(a)} + N_{2(g)}\uparrow \quad (10)$$

where k_{eff} is the effective rate constant for the electron-stimulated production of NH radicals from HN_3 (eq 10). In the present investigation the effective rate constant (k_{eff}) will remain constant since the X-ray flux is fixed. Consequently the concentration of the intermediate species (NH, NH_2, NH_3, N_3) can be treated on the basis of the steady-state approximation. Kinetic modeling of the elementary reaction steps postulated to comprise eq 9 leads to the following set of analytical expressions:[38]

$$[HN_3]_t = [HN_3]_0 \times e^{-4\,k_{eff}\,t} \quad (11)$$

$$[NH_4^+N_3^-]_t = {}^1/_4 \times (1 - e^{-4\,k_{eff}\,t}) \times [HN_3]_0 \quad (12)$$

$$[N_2]_t = (1 - e^{-4\,k_{eff}\,t}) \times [HN_3]_0 \quad (13)$$

Since any nitrogen (N_2) produced is expected to immediately desorb from the surface at 100 K, it will not contribute to the observed N(1s) XPS signal ($[N]_t$). Thus, the overall loss of N(1s) XPS intensity from the film as a function of X-ray irradiation time should follow the following functional form:

$$[N]_t = {}^1/_3 \times [N]_0 \times (2e^{-4\,k_{eff}\,t} + 1) \quad (14)$$

A comparison of the experimentally observed variation in N(1s) signal intensity and the best data fit calculated using eq 14, are shown as an insert in Figure 8, yielding a $k_{eff} = 0.162$ min^{-1}. The success of eq 14 in being able to model the loss of nitrogen under the influence of X-ray irradiation is therefore at least consistent with the proposed mechanism. In addition, the loss of nitrogen appears to arise solely from electron rather than thermally mediated processes, in accord with the constant temperature observed during irradiation.

Hydrazoic Acid Adsorption on Ice. Figure 4 shows that in contrast to the molecular adsorption of HN_3 on Au at 100 K (Figure 1), the initial interaction of HN_3 with the ice surface is dominated by deprotonation and N_3^- formation within the ice film (eq 1). The appearance of a band at 2043 cm^{-1}, prior to HN_3 exposure (Figure 4(a)) can be ascribed to the reaction between background HN_3 (residual from previous experiments) and the ice film. RAIRS experiments carried out using an MCT detector (Figure 7(b)) failed to reveal the presence of the hydronium ion, expected at ≈1750 cm^{-1}, presumably due to its broad and weak signal intensity.[23] The observation of a limiting N_3^- concentration (Figure 4, inset) upon prolonged HN_3 exposure suggests that the amount of azide formed is correlated with the thickness of the ice film. This assertion is supported by results of separate experiments on three different ice films shown in Table 4. Results from these studies indicate that the maximum concentration of azide ions observed, measured by the integrated area of the $\upsilon_a(N_3^-)$ mode, scales with the initial thickness of the ice film (measured by the integrated area of the O−H stretching mode). In each case the variation in $\upsilon_a(N_3^-)$ and υ_a(NNN) band intensity as a function of HN_3 exposure showed a similar variation to that shown in Figure 4, inset.

TABLE 4: Comparison of Maximum Azide Ion RAIRS Intensity Observed as a Function of Ice Film Thickness for Three Separate Films Exposed to ≈150 L HN_3 Using the Areas of the υ_s(O−H) and $\upsilon_a(N_3^-)$ IR Bands, Respectively

relative thickness of ice film (area of υ_s(O−H) band)	maximum azide concentration (area of $\upsilon_a(N_3^-)$ band)
1.0	0.49
0.96	0.47
0.69	0.10

Although the initial interaction of HN_3 with ice is dominated by ionization of the parent molecule, the appearance of intensity in the υ_s(NNN) stretching region and the observation of υ_s(N−H) as a shoulder on the water bands at 3143 cm^{-1} (Figure 4) indicate that molecular HN_3 is also present. Based on the ionization enthalpy and pK_a of HN_3 in water at STP, the degree of ionization at 100 K is predicted to be ≈0.85.[39] Despite the uncertainties inherent in this extrapolation, some of the molecular HN_3 observed in this early exposure regime could therefore be ascribed to $HN_{3(aq)}$. However, another potential source of HN_3 under these low-temperature conditions where molecular diffusion will be limited, could be the result of collisions between gas-phase HN_3 molecules with regions of the ice film that have already become saturated with azide ions.

Continued exposure of the ice film to HN_3 lead to deposition of a condensed multilayer, shown in Figure 4(c)−(f). In contrast to the smooth variation in the υ_a(NNN) peak position observed during adsorption of HN_3 on Au (Figure 1), the evolution of this same region during the interaction of HN_3 with ice suggests the presence of two distinct molecular HN_3 adsorbed states with peaks centered at ≈2153 cm^{-1} and ≈2177 cm^{-1}. Analysis of Figure 4(c)−(f) indicates that the lower frequency feature is populated preferentially. The presence of two distinct molecular environments for molecular HN_3 on ice becomes more evident during thermal annealing experiments of the HN_3/ice film (Figure 5).

On D_2O/H_2O ice films at 100 K, HN_3 adsorption produced no additional intensity in the 2308−2329 cm^{-1} region (Figure 6(b)), associated with the N−D stretching mode of DN_3.[15] Similarly, no isotopic H/D exchange was evidenced during sample annealing below 135 K, prior to HN_3 desorption (Figure 6(b) and (c)). Thus H/D exchange through the reaction, $HN_3 + D_2O \rightarrow DN_3 + HDO$, does not appear to be significant at these low temperatures.

Thermal Chemistry of the HN_3/Ice System. Adsorption of HN_3 on ice at 100 K, initially is dominated by azide ion formation followed by deposition of molecular HN_3 at longer exposures (Figures 4−7). During sample warming the first visible change in the ice/N_3^-/HN_3 film measured by RAIRS occurs at ≈130 K with an increase in the sharpness of the υ_s(N−H) mode at 3143 cm^{-1}. This can be ascribed to an irreversible phase change within the molecularly adsorbed HN_3.[15] In the same temperature region, two distinct bands associated with molecular HN_3 can be resolved in the υ_a(NNN)

region at 2177 cm^{-1} and 2153 cm^{-1}. The integrated area within the υ_a(NNN) region (2130−2190 cm^{-1}) remains virtually unchanged between 100 K and 130 K (Figure 5, inset) suggesting that these changes in the υ_a(NNN) region are driven by an increased mobility and/or structural changes within the HN_3/ice film.

Figure 4 shows that within the υ_a(NNN) region the 2177 cm^{-1} mode is populated only at longer HN_3 exposures (>10 min) after the concentration of adsorbed azide ions has reached a saturation value within the ice film. Thereafter population of the 2177 cm^{-1} mode continues to increase linearly as a function of HN_3 dosing time (Figure 4, inset) indicative of HN_3 molecules in a condensed/multilayer phase.

Desorption of molecular HN_3 from the multilayer state is complete by 157 K (Figures 5(e) and 6(e)) and is accompanied by an increase in the $\upsilon_a(N_3^-)$ band intensity (Figures 5(c)−(e) and 6(d)−(f) and insert). The absence of any new IR bands associated with ammonium azide ($NH_4^+N_3^-$) at 157 K, most notably the υ_3 mode at ≈3029 cm^{-1}, indicate that the increase in $\upsilon_a(N_3^-)$ band intensity is solely due to the production of $N^-_{3(a)}$. This increase in azide ion concentration can be ascribed to reactions between the ice surface and molecularly adsorbed, or gas-phase HN_3 molecules, the latter originating from the sample manipulator as the temperature increases. Irrespective of the origin of HN_3 molecules, the results shown in Figures 5 and 6 indicate that a greater capacity for adsorbed azide ions exists within the film at this higher temperature, possibly due to increased molecular/ionic diffusion and/or structural changes in the film. An alternative explanation which would also account for the observed increase in $\upsilon_a(N_3^-)$ band intensity could be due to rearrangement of azide ions within the film. According to the metal surface selection rule, the $\upsilon_a(N_3^-)$ band would increase in observed intensity if the change in the dipole moment associated with the vibration, became aligned preferentially parallel to the surface normal. This explanation is not favored, as there does not appear to be any a priori reason N_3^- would adopt a preferred orientation in these ice films.

During HN_3 adsorption on ice, the υ_a(NNN) mode at 2153 cm^{-1} is populated before the appearance of multilayer HN_3 (Figure 4). Consequently, this state at 2153 cm^{-1} (α-state) can be identified as either $HN_{3(aq)}$ or HN_3 molecules in close proximity to the ice/N_3^- film, the latter comprising a distinct "surface state." Evidence of distinct "surface states" for adsorbates on ice surfaces has previously been reported by Ogasawara et al. in a study of the adsorption and solvation of ammonia.[40] For those α-state HN_3 molecules, thermal and vibrational characteristics suggest a degree of hydrogen bonding with the ice film (i.e., $H_2O\cdots H-N_3$). The idea of a $N-H\cdots O$ hydrogen bond has also been used to explain the unusual solubility of HN_3 in ether.[41] The existence of hydrogen bonding on ice surfaces is consistent with the proposed interaction of molecular HCl[42] and HBr[23] with ice surfaces through the formation of $O\cdots H-Cl/Br$ hydrogen bonds. In the case of HCl, hydrogen bonding has also been shown to impart an additional degree of thermal stability.[42] It should be noted that intermolecular hydrogen-bonding has also been observed between HN_3 molecules leading to the formation of an open dimeric species.[26] The strength of this interaction, however, is expected to be much lower than that between HN_3 and H_2O, mainly because of the weakness of HN_3 as a hydrogen-bonding base.

In contrast to the condensed phase, desorption of α-state HN_3 molecules is complete by ≈180 K, and is accompanied by ammonium azide production prior to H_2O desorption. The presence of $NH_4^+N_3^-$ is evidenced by the appearance of new IR bands at 2855 cm^{-1}, 3029 cm^{-1}, and 3143 cm^{-1} (Table 2) as well as an increase in the IR peak position and intensity within the $\upsilon_a(N_3^-)$ region (Figure 5, inset). Results from experiments carried out using predominantly D_2O rather than H_2O ice films (Figure 6) are qualitatively consistent with those obtained using H_2O; notably the initial production of azide ions at 100 K, molecular desorption of HN_3 above 135 K, and production of ammonium azide by 180 K. The reactivity of the $H(D)N_3$/ice system is at least qualitatively consistent with the fact that aqueous HN_3 solutions have been known to explode when the HN_3 content exceeds 20%, illustrating the highly reactive nature of HN_3 in aqueous environments.[43]

SCHEME 1: Summary of Thermal and X-ray-Induced Reactions of Hydrazoic Acid Adsorbed on Amorphous Ice (Balanced equations are given in the Discussion section.)

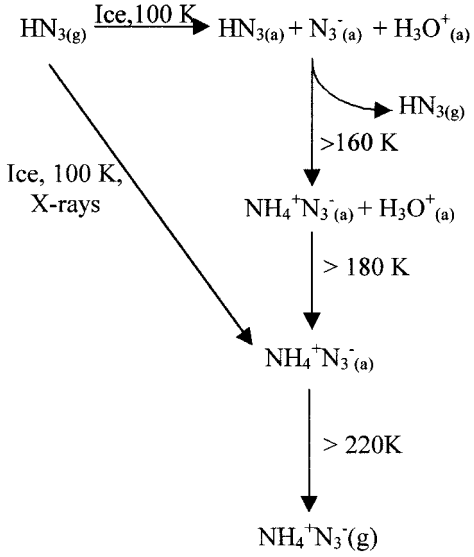

A summary of both the thermal and X-ray-induced chemistry of HN_3 adsorbed on an amorphous ice film at 100 K is shown schematically in Scheme 1.

Mechanism of $NH_4^+N_3^-$ Formation. $NH_4^+N_3^-$ production in the HN_3/ice system is postulated to occur via a mechanism analogous to the one proposed for the X-ray (secondary electron)-mediated reaction of HN_3 on Au (eq 4−9), with the exception that NH radicals are now produced from thermal decomposition:

$$HN_{3(a)} \xrightarrow{\Delta} NH_{(a)} + N_{2(g)}\uparrow \qquad (15)$$

The source of NH radicals is postulated to originate from thermally activated NN−NH bond cleavage of α-state HN_3 molecules. This new reactive channel is proposed to arise as a consequence of hydrogen bonding, which could weaken the NN−NH bond and/or lower the activation energy associated with reaction 15. In principle HN_3 could decompose via either NN−NH or NNN−H bond cleavage, to produce NH/N_2 or H/N_3, respectively. However, as has been pointed out by previous researchers, breaking the NN−NH bond to form NH and N_2 is much more thermodynamically favorable, compared with the energy required to break the NNN−H bond, which is only observed on surfaces much more reactive toward HN_3 e.g., C(100).[10] The absence of ammonium azide formation during any annealing experiments on Au (Figure 2) argues strongly that H_2O is necessary for NH radical formation and hence ammonium azide production. Once formed, $NH_4^+N_3^-$ remains

stable until ≈230 K consistent with the desorption characteristics of the same species observed by Heidberg et al.[9]

Ammonium azide formation could in principle also arise from reactions initiated between N_3^- and the ice film during sublimation. However, the close correlation between HN_3 desorption from the α-state and the increase in $\upsilon_a(N_3^-)$ band intensity (Figure 5, inset) suggests that reactions associated with HN_3 are at least in part responsible for ammonium azide formation. This assertion is also supported by a comparison of Figure 5(e) and (f) as well as Figure 7(c) and (d) demonstrating that a significant amount of ammonium azide is formed during thermal annealing of the ice/N_3^-/HN_3 film but prior to H_2O desorption. Furthermore, despite the presence of an ice film composed primarily of D_2O the majority of the ammonium azide produced is still $NH_4^+N_3^-$ (Figure 6). This observation suggests that ammonium azide formation is initiated from reactions between nitrogen-containing species derived from molecular HN_3, such as reactions 5−7, rather than those between azide ions and the ice film which would be expected to produce ND containing ammonium azide as the majority species.

The limited amount of H/D exchange evidenced in Figure 6 is hypothesized to result from reactions initiated after the formation of $NH_4^+N_3^-$ but before the ice/water film sublimes, for example:

$$NH^+_{4(a)} + D_2O_{(a)} \rightarrow NH_3D^+_{(a)} + HDO_{(a)} \qquad (16)$$

However, other reactions could also account for the H/D exchange observed before the formation of ammonium azide. For example:

$$NH_{3(a)} + D_3O^+_{(a)} \rightarrow NH_3D^+_{(a)} + D_2O_{(a)} \qquad (17)$$

$$NH_{(a)} + D_2O_{(a)} \rightarrow NHD_{(a)} + OH_{(a)} \qquad (18)$$

eq 18 has previously been shown to have an enthalpy of reaction of -57.5 kJ mol^{-1} arguing for the possibility of H/D exchange through this mechanism.[3]

V. Conclusions

Hydrazoic acid was found to adsorb molecularly on Au at 100 K. Annealing lead predominantly to molecular HN_3 desorption, although RAIRS and XPS data support the idea of a more strongly bound state which at higher temperatures is responsible for the production of a Au−N(H) bond. In contrast to the HN_3/Au system, the initial interaction of hydrazoic acid with an ice film at 100 K is dominated by azide ion formation until a saturation concentration is reached. At higher exposures HN_3 adsorbs molecularly, although another distinct molecular state was also observed, attributed to hydrogen bonding between HN_3 and H_2O. Annealing the HN_3/ice system resulted in formation of ammonium azide ($NH_4^+N_3^-$). Above 180 K, $NH_4^+N_3^-$ was identified in RAIR and XPS data as the only species present. Formation of $NH_4^+N_3^-$ was also observed following X-ray irradiation of hydrazoic acid on Au or ice surfaces. The mechanism proposed for the formation of $NH_4^+N_3^-$ is based on the thermal or secondary electron-induced formation of NH radicals and was found to be consistent with an overall net reaction of: $4HN_{3(a)} \rightarrow NH_4^+N^-_{3(a)} + 4N_{2(g)}\uparrow$

Acknowledgment. The authors express their gratitude to A. J. Wagner for making the XPS measurements on the interaction of HN_3 with Au at room temperature. We also thank the Materials Research Science and Engineering Center surface analysis laboratory, funded through the National Science Foundation, for use of the 5400 Phi XPS system and Dr. Francois Reniers (Université Libre de Bruxelles) for providing the Au-coated microscope slides. This work was supported in part by the Petroleum Research Fund (PRF # 35281-G5,6G) administered by the American Chemical Society and through a National Science Foundation CAREER grant (#9985372).

References and Notes

(1) Lee, T. H.; Colton, R. J.; White, M. G.; Rabalais, J. W. *J. Am. Chem. Soc.* **1975**, *97*, 4845.
(2) Colton, R.; Rablias, J. W. *J. Chem. Phys.* **1976**, *64*, 3481.
(3) Hack, W.; Mill, T. *J. Phys. Chem.* **1991**, *95*, 4712.
(4) Schlie, L. A.; Wright, M. W. *Anal. Chem.* **1990**, *53*, 665.
(5) Chu, J. C. S.; Bu, Y.; Lin, M. C. *Surf. Sci.* **1993**, *284*, 281.
(6) Tindall, C.; Hemminger, J. C. *Surf. Sci.* **1995**, *330*, 67.
(7) Russell, J. N.; Bermudez, V. M.; Leming, A. *Langmuir* **1996**, *12*, 6492.
(8) Porezag, D.; Pedersen, M. R.; Liu, A. Y. *Phys. Rev. B* **2000**, *61*, 13230.
(9) Heidberg, J.; Hustedt, M.; Opperman, J.; Paszkiewiz, P. *Surf. Sci.* **1996**, *352−354*, 447.
(10) Thoms, B. D.; Russell, J. N. *Surf. Sci.* **1995**, *337*, L807.
(11) Carlo, S. R.; Wagner, A. J.; Fairbrother, D. H. *J. Phys. Chem. B* **2000**, *104*, 6033.
(12) Wagner, A.; Torres, J.; Fairbrother, D. H. *J. Phys. Chem. B* **2000**, *104*, 3291.
(13) *The Handbook of X-ray Photoelectron Spectroscopy*; Perkin-Elmer Corporation: 1979.
(14) AugerScan; 2.4 ed.; RBD Enterprises Inc:.
(15) Dows, D. A.; Pimentel, G. C. *J. Chem. Phys.* **1953**, *23*, 1258−1263.
(16) Bradley-Moore, C.; Rosengren, K. *J. Chem. Phys.* **1966**, *44*, 4108.
(17) Rosengren, K.; Pimental, G. C. *J. Chem. Phys.* **1965**, *43*, 507.
(18) Gray, P.; Waddington, T. C. *Trans. Faraday Soc.* **1957**, 901.
(19) Shimanouchi, T. *J. Phys. Chem. Ref. Data 6* **1977**, 993.
(20) Schaff, J. E.; Roberts, J. T. *J. Phys. Chem.* **1996**, *100*, 14151.
(21) Dows, D. A.; Whittel, E.; Pimental, G. C. *J. Chem. Phys.* **1955**, *23*, 1475.
(22) Bu, Y.; Lin, M. C. *Surf. Sci.* **1994**, *301*, 118.
(23) Carlo, S. R.; Grassian, V. H. *J. Phys. Chem. B* **2000**, *104*, 86.
(24) Horn, A. B.; Banham, S. F.; McCoustra, R. S. *J. Chem. Soc., Faraday Trans.* **1995**, *91*, 4005.
(25) Raimbault, G.; Romain, F.; Lautie, A. *J. Raman Spectrosc.* **1992**, *23*, 147.
(26) Pimentel, G. C.; Charles, S. W.; Rosengren, K. *J. Chem. Phys.* **1966**, *44*, 3029.
(27) Krejzler, J.; Siekierski, S. *J. Soln. Chem.* **1995**, *24*, 253.
(28) Hollins, P.; Pritchard, J. *J. Prog. Surf. Sci.* **1985**, *19*, 275.
(29) Dalmia, A.; Savinell, R. F.; Liu, C. C. *J. Electrochem. Soc.* **1996**, *143*, 1827.
(30) Clark, D. T.; Brenan, W. J. *J. Electron. Spectrosc. Relat. Phenom.* **1986**, *41*, 399.
(31) Wheeler, D. R.; Pepper, S. V. *J. Vac. Sci. Technol.* **1982**, *20*, 226.
(32) Labinis, P. E.; Graham, R. L.; Biebuyck, H. A.; Whitesides, G. M. *Science* **1991**, *254*, 981.
(33) Becker, E. D.; Pimental, G. C.; Thiel, M. V. *J. Chem. Phys.* **1957**, *26*, 145.
(34) Tokue, I.; Ito, Y. *Chem. Phys.* **1983**, *79*, 383.
(35) Fukui, K.; Fujita, I.; Kuwata, K. *J. Phys. Chem.* **1977**, *81*, 1252.
(36) Tsunashima, S.; Hamada, J.; Hotta, M.; Sato, S. *Bull. Chem. Soc. Jpn.* **1980**, *53*, 2443.
(37) Kitamura, T.; Tsunashima, S.; Sato, S. *Bull. Chem. Soc. Jpn.* **1981**, *54*, 55.
(38) The exponential power of $-4k_{eff}t$ arises from the steady-state analysis of the reactions leading to the formation of ammonium azide, e.g., $d[NH]/dt = 0$.
(39) Smith, R. M.; Martell, A. E. *Critical Stability Constants*; Plenum: New York, 1982; Vol. 4.
(40) Ogasawara, J. *J. Chem. Phys.* **2000**, *112*, 8229.
(41) Buswell, A. M.; McMillan, G. W.; Rodebush, W. H.; Wall, F. T. *J. Am. Chem. Soc.* **1939**, *61*, 2809.
(42) Graham, J. D.; Roberts, J. T. *J. Phys. Chem.* **1994**, *98*, 5974.
(43) Joebilius, H. K. *Ullman's Encyclopedia of Industrial Chemistry*; Schaff, H.-D., Ed.; VCH: Weinheim, 1989; Vol. A13, p 193.
(44) Benedict, W. S.; Plyer, E. K. *Can. J. Phys.* **1957**, *35*, 1235.
(45) Eyster, E. H.; Gillette, R. H. *J. Chem. Phys.* **1968**, *72*, 459.
(46) LeBorgne, C.; Illien, B.; Beignon, M.; Chabnel, M. *Phys. Chem. Chem. Phys.* **1999**, *1*, 4701.